Chaos

AIP Publishing

Sol-gel transition programmed self-propulsion of chitosan hydrogel

Pawan Kumar,[1] Dezső Horváth,[2] and Ágota Tóth[1]
[1)]*Department of Physical Chemistry and Materials Science, University of Szeged, Rerrich Béla tér 1., Szeged, H-6720, Hungary.*
[2)]*Department of Applied and Environmental Chemistry, University of Szeged, Rerrich Béla tér 1., Szeged, H-6720, Hungary.*

(*Electronic mail: atoth@chem.u-szeged.hu)

(Dated: 17 May 2022)

Active soft materials exhibit various dynamics ranging from boat pulsation to thin membrane deformation. In the present work, *in situ* prepared ethanol-containing chitosan gels propel in continuous and intermittent motion. The active life of the organic material loaded to the constant fuel level follows a linear scaling, and its maximal velocity and projection area decrease steeply with the chitosan concentration. A thin propelling platelet forms at low polymer content, leading to the suppression of intermittent motion. Moreover, the fast accelerating thin gels can split into a crescent and circular-like shape or fission into multiple asymmetric fragments.

Self-propulsion behavior is the core of living organisms, making them perform distinct tasks in coordination and survival strategies that assist in their evolution. Energy transduction yields the functioning of biological systems under isothermal equilibria. In an artificial active system, the conversion of chemical energy into kinetic energy self-propels the object due to the asymmetry in the interfacial tension around its locality. The mode of spontaneous agitation relies on the design of the motor and the size of the container. In this work, a new way to explore the self-propelled motion of hydrogel is studied. A polymer boat is created *in situ* which exhibits rotational and/or translational motion. It is shown that the gel deforms into various shapes by varying the composition of the infused fuel and the polymer solution.

I. INTRODUCTION

Dissipative systems self-organize to various spatiotemporal structures and produce autonomous activities.[1] Active material moves on its own by consuming chemical,[2–5] electromagnetic,[6] electrical energy,[7–9] or light[10–12]. Various mechanisms such as Marangoni effect,[13,14] electroosmosis,[9] bubble ejection,[15,16] dielectrophoresis[7] have been proposed to direct the propulsion activities. The well-known interfacial phenomenon, the so-called Marangoni effect, drives the object towards the higher surface tension caused by chemical or thermal gradients. Over the last few decades, a wide range of artificial solid, liquid, and gel-based motors[1] and quantitative parameter estimation[17] has been investigated and gained the immense attraction of scientists. The spontaneous motion of motors mimics the behavior of living organisms. Several practical applications are being explored, from drug delivery[18] to bio-actuators[19] and from sensors for toxicity detection[20] to chemical spills for environmental remediation[21].

Designing new self-propelled machines is always a topic of interest in nonlinear science and technical applications. The underlying dynamics of motors include translational, rotational, and spinning motion. Contemporary research has also identified periodic oscillations in a string of camphor-infused disks,[22] filament-like undulatory and vertical oscillatory motions[23]. Interestingly, the polymer gels' flexible, soft and swelling features make them perfect candidates to fabricate high-tech programmable motors. The gel-based self-motion on the water surface generally occurs either by spreading solvents due to the Marangoni effect or by continuously releasing organic molecules via osmotic and hydrostatic pressure from the gel. The latter mechanism produces spontaneous motion of amphiphilic polymer gels[24] and the spreading of the infused organic solvents generates periodic motion of polyacrylamide hydrogel contained in plastic tubing,[25] and spinning motion in a photo-patternable poly-N-isopropyl acrylamide gel[26].

The instability induced by the interfacial tension gradients deforms and splits the active droplets.[27–30] The well-known examples include the formation of tears on the wall of the wine glass[31] and the erratic splitting of an alcohol droplet on an aqueous surface[30]. Mechanical stress on the gels can also deform their shapes and induce cracking patterns and fracturing.[32] It has been found that the formation of a gel layer of tetradecane droplet containing palmitic acid on a stearyl trimethyl ammonium chloride aqueous solution forms blebbing dynamics and fission.[33–36]

We report a polysaccharide chitosan gel-based motor by implementing a new approach via sol-gel transition technique. The propulsion behavior exhibits translational and rotational motion, and the gel develops complex structure, even symmetric and erratic gel splitting can take place. The polymer concentration along with the infused fuel amount controls the motion dynamics and the structure deformations.

II. EXPERIMENTAL

Analytical grade reagents CH_3COOH (99 – 100 %), ethanol (99 – 100 %), NaOH (pellets) were purchased from VWR, and polysaccharide medium molecular weight chitosan (CS) was obtained from Sigma-Aldrich (448877). The pre-gel CS sol (0.58 – 3.0 w/V % CS(sol)) in 0.2 M CH_3COOH, NaOH (3.0 M) and ethanol (86 V/V %) solutions were prepared with

deionized water (Purite 300).

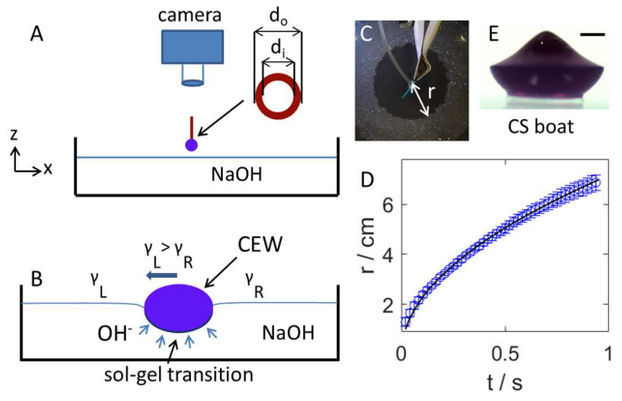

FIG. 1. (Color online). (A-B) Schematic diagram of self-propelled chitosan gel. (C) Top view image of ethanol drop expansion with field view: 16.14 × 16.87 cm^2 and (D) temporal evolution of the radius of the ethanol drop. (E) Side view of the chitosan boat built from 3.0 w/V % CS(sol) concentration with R = 3.0 and V_w = 0 mL. Scale bar: 1 mm.

To observe the motion of the CS gel boat, 4 mL of CS-ethanol-water (CEW) solutions were mixed in various compositions (see Table S1) with 0.008 w/V % methylene blue (Reanal) to aid visualization. For presentation purposes, the chitosan-ethanol volume ratio was calculated as $R = (V_{CS} + V_w)/V_{EtOH}$, where V_{CS}, V_w and V_{EtOH} represent the volume of acidic chitosan sol, water, and ethanol (86 V/V %), respectively. All solutions were stirred for 2 hours and stored overnight at room temperature.

Figure 1A shows the schematic diagram of the experimental setup, where a glass container of dimension 22 × 22 × 5 cm^3, containing 300 mL alkaline solution, was placed horizontally. A fresh drop of *CEW* solution was dripped from 9.2 mm far from the alkaline surface using a peristaltic pump (Ismatec Reglo) through the Tygon tube ($i.d.$ = 1.42 mm) and plastic needles (d_i = 1.65 mm or 2.5 mm). White chalk powder was used for tracing the drop expansion.

Videos were recorded with a digital camera (25 frames/s), CCD-Vivitar camera (15 frames/s), or Osmo action camera (240 frames/s) by projecting above the container, illuminated with an LED light source. The images of the gelated bead were captured using a CCD camera equipped with Vivitar lens or a microscope (Nikon Eclipse Ts2R) coupled with a CCD camera (Nikon LVTV). The data were analyzed using ImageJ and MatLab 2021 softwares. All experiments were performed at temperature 24 ± 1 ^{o}C.

III. RESULTS AND DISCUSSION

When a CEW droplet is placed on the sodium hydroxide solution surface, as shown in Figure 1B, a thin chitosan gel layer forms immediately between the interface of the acidic and alkaline solutions. The gel thickens/strengthens over time as the mobile hydroxide ions diffuse into the acidic chitosan sol creating a gel bead of around 4–10 mm in diameter. The ethanol in the droplet spreads out on the NaOH surface (Fig. 1C). Its expansion is measured separately by dripping a CS-free droplet with R = 3 and V_w = 3 mL on the alkaline surface. The radius growth (see Fig. 1D), scales with time as

$$r = kt^{\alpha}\ , \tag{1}$$

where $k = 51.19 \pm 3.82$ cm^2 s^{-1} and $\alpha = 0.50 \pm 0.02$, similarly to the diffusional spreading of volatile compounds like camphoric acid on water surface.[37]

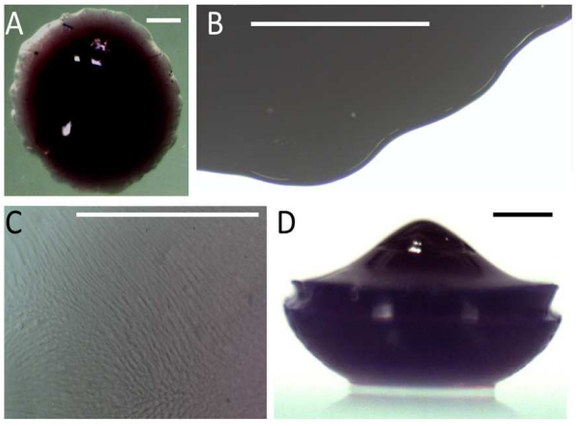

FIG. 2. (Color online). (A) Top view of the gel, (B) top view near boundary and (C) central view of the gelated bead for the CS(sol) concentration of 1.5 w/V %. (D) Two layers of the bead at 3 w/V % CS(sol). Scale bar = 1 mm. The compositions are used: R = 3, V_w = 0 mL.

The gel bead formed during the reaction is taken out of the solution and kept on the glass substrate for the visualization of its structure. For low CS concentrations in the gel, the upper and lower side of the gel bead maintain the convex and concave shapes, respectively. The gel is sufficiently soft, so when it makes contact with the glass it can adhere to it. However, a rigid structure develops at high CS concentrations as shown in Fig. 1E. The upper surface becomes conical, resulting in a boat-like structure due to the evaporation of ethanol during the time scale of the experiments. The top view of the CEW droplets looks circular (Fig. 2A), regardless of their outer edge. A close inspection of the gelated bead reveals that the outer edge is wavy, typical for evaporation (Fig. 2B), while at the central core irregular ridge-like patterns evolve (Fig. 2C). When the gel boat with high CS concentration is left one hour in the alkaline solution, the diffusion of OH^- creates "two-level" boats (Fig. 2D), similar to multilayer hydrogels[38].

As the CEW droplet contacts with the alkaline solution, besides the gel formation, the Marangoni effect—due to the ethanol spreading—generates the motion of the gel instantly. The speed of the boat at a given time, defined as

$$v_i = \sqrt{(x_{i+1} - x_i)^2 + (y_{i+1} - y_i)^2}/\Delta t\ , \tag{2}$$

characterizes the dynamic activities, where i represents the frame number, (x, y) coordinates are the centroid of the bead

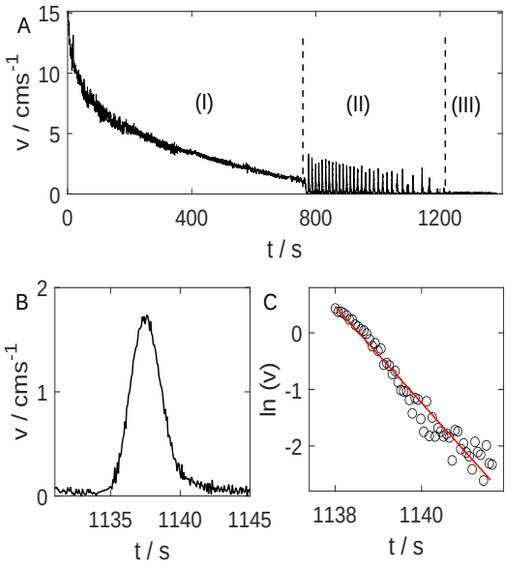

FIG. 3. (Color online).(A) Speed evolution of the self-propelled CS gel. (B) A spike of the intermittent state and (C) ln(v) as a function of time. The red line indicates the linear fit. The concentration of CS(sol) is 2.0 w/V% with $V_w = 0$ mL and $R = 3$.

and Δt expresses the time interval between the frames. The speed evolution in Figure 3A indicates that before reaching a quiescent state (III), the gel bead exhibits continuous (I) and intermittent (II) motion. The collision of the gel with the wall decreases its speed, therefore the data near the container boundaries are eliminated manually by checking the entire speed profile (Figure S1). The speed of the bead in region (I) decreases sharply due to the quickly decreasing ethanol supply rate. The propulsion begins in a straight path, which, after hitting the boundaries, may switch to a circular one (Movie S1). The development of circular motions are expected due to the wavy patterns on the gel and the slowing down of the propulsion.

In the second stage (II), the bead exhibits stop and run motion (Movie S2), producing spikes in the velocities in Figure 3A. Due to the depletion of ethanol, the distance traveled by the diffusion of ethanol from the central to the outer region increases, which increases the interspike period T_p with time. The T_p follows a linear scaling with the rest state T_r (Figure S2) with slope of 0.94 ± 0.03, which supports that on average, the variation in propulsion time of spikes is insignificant. In region II, the gel bead accelerates abruptly at the beginning of spiking as shown for an example case in Figure 3B. The speed of the gel boat reaches a maximum and then it decreases exponentially (Fig. 3C), indicating a relaxation-like motion. The frictional coefficient of the gel bead (μ) can be calculated by assuming that no driving force acts on it, and the initial speed $v(0)$, identified as the maximum speed, exponentially decreases as a function of time, i.e.,

$$v(t) = v(0)e^{-\frac{\mu}{m}t}\ , \tag{3}$$

where m is the mass of the bead ($\sim$25 mg, see Table S1). From the slope of the fitted line in Figure 3C, the frictional coefficient is estimated to be $(2.08 \pm 0.05) \times 10^{-5}$ N m^{-1} s. For a given R, the formation of the thin gel can be comparable to an elastic sheet at low concentrations of chitosan. The CS membrane is flexible and upon collision with the container wall, the gel adheres to the glass surface and produces an oscillatory motion like pendulum (Movie S3) with increasing period of the oscillations due to the depletion of ethanol (Figure S3).

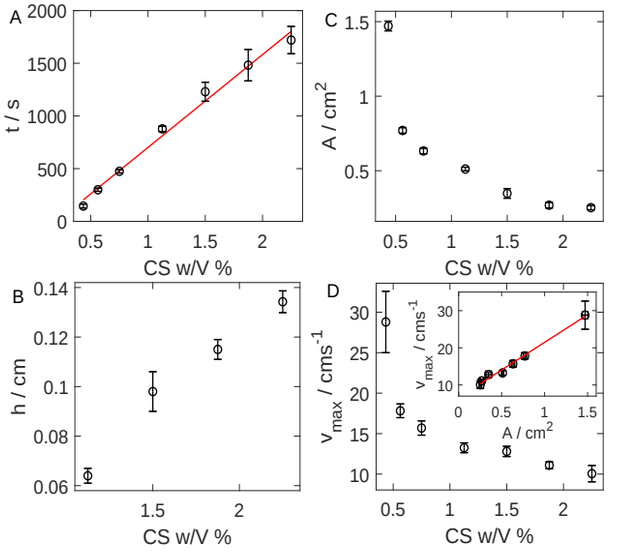

FIG. 4. (Color online). (A) Propulsion time of the gel and the gel characteristics such as (B) depth h, (C) projection area A, and (D) maximal velocity v_{max} as a function of CS concentrations with $R = 3$ and $V_w = 0$. The red lines correspond to the linear fittings.

The active time of the bead increases linearly as a function of CS concentrations (see Figure 4A) at constant R and constant amount of ethanol. Increasing the chitosan concentration increases the viscosity of the sol (Table S1) and hence increases the cohesive force between the polymer chains. Because of that, the chains are tightly packed at high concentrations causing a slower supply rate of the infused fuel in the droplet under which the bead stays active for a longer time. The physical characteristic of the droplet, the submerged depth h, increases with concentration as shown in Fig. 4B due to the increasing polymer density. The top projection area A, however, decreases steeply as a function of the CS concentration (Fig. 4C) because of the increasing cohesive force in the polysaccharide sol. The maximal speed is determined by considering the largest speed values in the first ten seconds of the experiments. Figure 4D shows that the maximal speed decreases abruptly as the concentration of polymer increases and follows a linear tendency with the projection area (see the inset figure). Upon increasing the area of the ethanol-loaded gel, the drag force and the supply rate increase. The drag force decreases the speed, but the supply rate increases the concentration gradients and increasing the maximal propulsion speed. The rise in the maximal speed with A reveals the

dominating effects of the interfacial tension gradients on the acceleration of the bead.

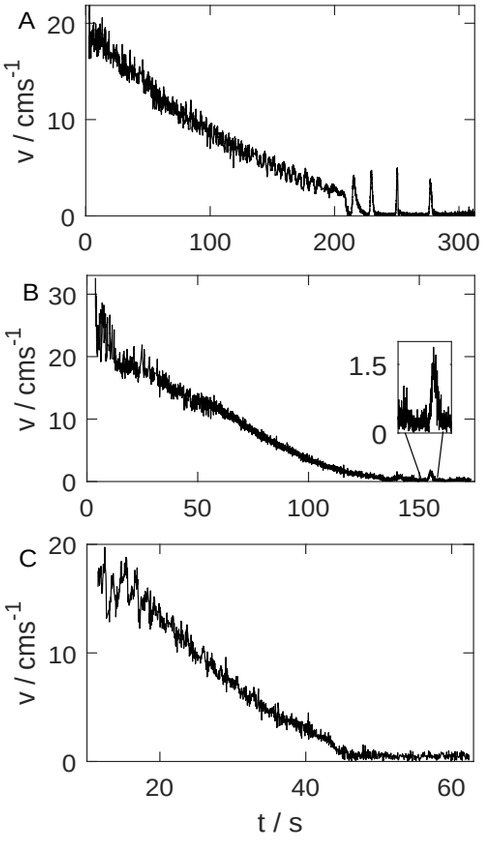

FIG. 5. Speed evolution of the gel for the compositions of (A) $R = 3$, $V_w = 0$ mL, (B) $R = 1$, $V_w = 0$ mL, (C) $R = 3$, $V_w = 1$ mL. The chitosan sol concentration is 0.75 w/V %.

The variation of the fuel amount with respect to the polymer content, i.e, R and V_w, controls the dynamics and the shapes of the gel. The speed evolution in Figure 5A corresponding to $R = 3$ and $V_w = 0$ mL ($d_i = 1.65$ mm) shows the continuous and intermittent motion of the circular bead. Further increasing the fuel amount, thus decreasing R to 1, we find that chitosan droplet forms with an asymmetric shape and exhibits rotational motion. Figure 5B displays that the bead sustains the active state up to 155 ± 16 s and significantly suppresses the intermittent region. Comparing the two cases, we find that the circular-like bead has a sudden, steep transition from continuous to intermittent mode, while the asymmetric shape has a monotonic. Furthermore, the maximal velocity of 17.82 ± 0.85 cm s^{-1} of the circular bead increases to 26.58 ± 3.15 cm s^{-1} for the asymmetric gel, but the spiking speed decreases from 4.42 ± 0.45 cm s^{-1} to 1.67 ± 0.13 cm s^{-1}. When a droplet with the composition of 0.75 w/V% CS(sol), $V_w = 1$ mL and $R = 3$ ($d_i = 2.5$ mm) is placed on the alkaline surface, the projection area of the gel increases. A sheet-like circular thin membrane ruptures the edges, causing deformation to an asymmetric shape and leading to a movement along a ring pattern (Movie S4). The speed, illustrated in Fig. 5C, shows that the continuous motion reaches the quiescent state, resulting in the complete suppression of spiking events.

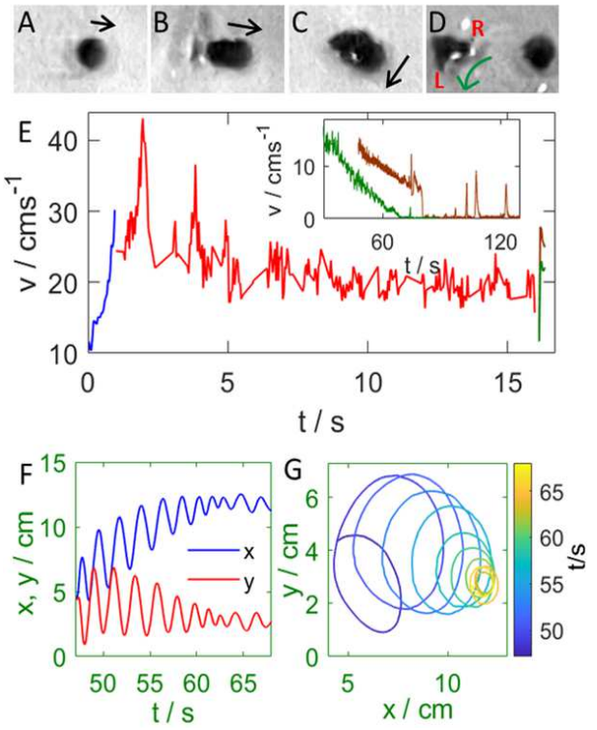

FIG. 6. (Color online). (A-D) Top-view images illustrate the shape transition. Field of view: 3.83×2.40 cm^2. (E) Speed evolution as a function of time. (F) Oscillatory motion of the crescent gel and (G) trajectories of the rotational dynamics. CS(sol): 0.75 w/V% with $R = 0.6$ and $V_w = 0$.

Increasing the ethanol amount tends to deform the shape of the organic droplet. Image sequence in Figure 6A-D renders the transition of the gel shape for a given composition of $R = 0.6$ and $V_w = 0$. When the droplet falls from the needle ($d_i = 2.5$ mm) on the alkaline, it forms a circular shape (Fig. 6A), and a thin layer separates the alkaline and polymer electrolytes. The propulsion speed sharply rises, depicted by the blue curve in Fig. 6E, but the upper solution of the organic drop stays in the near-rest state due to Newton's first law. This process spreads the upper solution backward and immediately creates a new gel layer attached to the initial formed gel layer resulting in an elliptical shape (Figure 6B). The further fast propulsion speed (red curve in Fig. 6E) expands the boundary of the gel (Fig. 6C), while the fuel consumption decreases the speed and the asymmetric shape produces the rotational dynamics. Later, the membrane splits into circular and asymmetric, crescent-like pieces, as shown in Fig. 6D. The length of the left (L) side of the asymmetric gel is shorter and thinner than the right (R) side, and the green arrow in Fig. 6D denotes the anticlockwise direction of the gel motion. The speed of the crescent shaped gel, shown by green in the inset of Figure 6E, monotonically reaches the intermittent zone. The circu-

lar piece also exhibits rotational motion, but the collision with and the adhesivity to the boundaries trap the gel and affect its dynamics. Figure 6F represents the oscillatory behavior of crescent gel. The color coded trajectory (Fig. 6G) in the later stage of the continuous motion displays the reduction in the size of the ring diameter with time, indicating the smooth transition from the continuous to the intermittent zone.

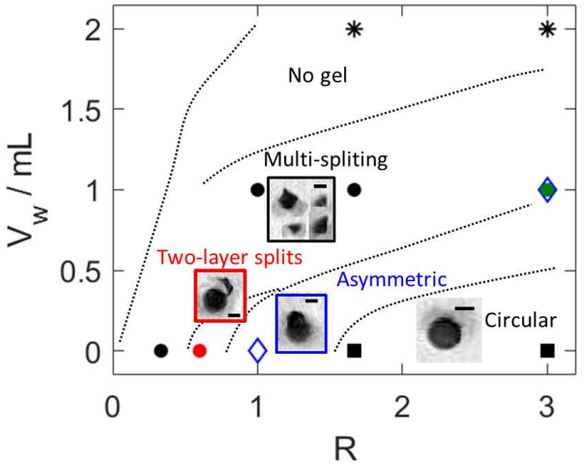

FIG. 7. (Color online). The dynamical phase diagram of the different growth regimes, guided by the black dotted lines. The needle inner diameter is used 1.65 mm and CS(sol) concentration is 0.75 w/V%. Scale bar: 5 mm.

We have summarized the qualitative picture of the observed shapes and dynamics of the active soft material in Figure 7. The shapes can be assigned to three distinct regions: circular (square markers), asymmetric (diamond markers), and splitting (circular markers). For the last case, the number of fragments increases, but the time of fracture occurrence decreases on decreasing R or increasing V_w, i.e., increasing the amount of the fuel or decreasing the polysaccharide concentration in the gel. Multi-splitting produces different shapes, and the dynamics of the individual fragments depend on their shape and the fuel amount in the gel. For example, for high fuel level with R = 1/3, V_w = 0 mL, and 0.75 w/V% CS sol, the large fragments can spike even with speed of 13.1 $\pm$ 0.2 cm s^{-1} (see Figure S4). Moreover, fission into multiple tiny particles are observed at high V_w. Further increase of the water in the CEW droplet, however, lowers the chitosan concentration so much that gel formation can not take place.

IV. CONCLUSIONS

We have designed a bio-inspired artificial system where self-propulsion activities are shown for ethanol-containing chitosan hydrogels. A dynamic transition from continuous to intermittent modes of motion has been observed, where the control of the stop-run motion is attained for varying the polymer concentration and the amount of the fuel in the polysaccharide. The expansion of the gel can induce splitting into fragments of distinct structural shapes.

Future studies can be aimed to explore the collective phenomena of chitosan beads and boats. The complexation of various metal ions with chitosan can modify the membrane properties, which may assist in manufacturing a smart motor for technical applications. The attractive-repulsive interaction of droplets can be controlled by appropriately selecting metal ions and tuning the solvent composition. It is possible to govern the various nonlinear phenomena and dynamic patterns that mimic the coordinating behavior of living organisms.

Moreover, the self-propelling droplet induces chemical gradients on both sides of the chitosan membrane and generates an electric potential as was shown in our previous work,[39] for self-organized tubular membranes. We believe that the present work can pave the way for future studies in advancing energy-based chemical motors.

V. SUPPLEMENTARY MATERIAL

The solution compositions, further figures on histograms and oscillatory dynamics of beads, and the temporal evolutions of gel speeds, along with videos on the various motion types of the gel beads are found in the supplementary material.

VI. ACKNOWLEDGEMENTS

This paper is dedicated to Prof. Richard Field of the FKN mechanism on his 80th birthday. This work was supported by the National Research, Development and Innovation Office (Grant No. K138844) and by the Ministry of Innovation and Technology of Hungary from the National Research, Development and Innovation Fund (TKP2021-NVA-19).

VII. CONFLICT OF INTEREST

The authors have no conflicts to disclose.

VIII. DATA AVAILABILITY

The data that support the findings of this study are available from the corresponding author upon reasonable request.

IX. REFERENCES

[1] V. Pimienta and C. Antoine, "Self-propulsion on liquid surfaces," Curr. Opin. Colloid Interface Sci. **19**, 290–299 (2014).
[2] T. Mitsumata, K. Ikeda, J. P. Gong, and Y. Osada, "Solvent-driven chemical motor," Appl. Phys. Lett. **73**, 2366–2368 (1998).
[3] Y. Xu, N. Takayama, H. Er, and S. Nakata, "Oscillatory motion of a camphor object on a surfactant solution," J. Phys. Chem. B **125**, 1674–1679 (2021).
[4] S. Nakata, M. Yoshii, Y. Matsuda, and N. Suematsu, "Characteristic oscillatory motion of a camphor boat sensitive to physicochemical environment," Chaos **25**, 064610 (2015).

[5]J. Sharma, I. Tiwari, D. Das, P. Parmananda, V. S. Akella, and V. Pimienta, "Rotational synchronization of camphor ribbons," Phys. Rev. E **99**, 012204 (2019).
[6]M. C. Hoang, K. T. Nguyen, V. H. Le, J. Kim, E. Choi, B. Kang, J.-O. Park, and C.-S. Kim, "Independent electromagnetic field control for practical approach to actively locomotive wireless capsule endoscope," IEEE Trans. Syst. Man Cybern.: Syst. **51**, 3040–3052 (2019).
[7]O. D. Velev, B. G. Prevo, and K. H. Bhatt, "On-chip manipulation of free droplets," Nature **426**, 515–516 (2003).
[8]G. Loget and A. Kuhn, "Propulsion of microobjects by dynamic bipolar self-regeneration," J. Am. Chem. Soc. **132**, 15918–15919 (2010).
[9]S. T. Chang, V. N. Paunov, D. N. Petsev, and O. D. Velev, "Remotely powered self-propelling particles and micropumps based on miniature diodes," Nat. Mater. **6**, 235–240 (2007).
[10]A. Yucknovsky, B. B. Rich, A. Westfried, B. Pokroy, and N. Amdursky, "Self-propulsion of droplets via light-stimuli rapid control of their surface tension," Adv. Mater. Interfaces **8**, 2100751 (2021).
[11]M. Ibele, T. E. Mallouk, and A. Sen, "Schooling behavior of light-powered autonomous micromotors in water," Angewandte Chemie **121**, 3358–3362 (2009).
[12]W. Duan, R. Liu, and A. Sen, "Transition between collective behaviors of micromotors in response to different stimuli," J. Am. Chem. Soc. **135**, 1280–1283 (2013).
[13]Y. Sumino, N. Magome, T. Hamada, and K. Yoshikawa, "Self-running droplet: Emergence of regular motion from nonequilibrium noise," Phys. Rev. Lett. **94**, 068301 (2005).
[14]N. J. Suematsu, Y. Miyahara, Y. Matsuda, and S. Nakata, "Self-motion of a benzoquinone disk coupled with a redox reaction," J. Phys. Chem. C **114**, 13340–13343 (2010).
[15]S. Nakata, M. Nomura, H. Yamamoto, S. Izumi, N. J. Suematsu, Y. Ikura, and T. Amemiya, "Periodic oscillatory motion of a self-propelled motor driven by decomposition of h2o2 by catalase," Angew. Chem. **129**, 879–882 (2017).
[16]Q. Wang, P. Knoll, and O. Steinbock, "Self-propelled chemical garden tubes," J. Phys. Chem. B (2021).
[17]N. J. Suematsu, T. Sasaki, S. Nakata, and H. Kitahata, "Quantitative estimation of the parameters for self-motion driven by difference in surface tension," Langmuir **30**, 8101–8108 (2014).
[18]D. Kagan, R. Laocharoensuk, M. Zimmerman, C. Clawson, S. Balasubramanian, D. Kang, D. Bishop, S. Sattayasamitsathit, L. Zhang, and J. Wang, "Rapid delivery of drug carriers propelled and navigated by catalytic nanoshuttles," Small **6**, 2741–2747 (2010).
[19]V. Chan, H. H. Asada, and R. Bashir, "Utilization and control of bioactuators across multiple length scales," Lab Chip **14**, 653–670 (2014).
[20]Y. Zhang, K. Yuan, and L. Zhang, "Micro/nanomachines: from functionalization to sensing and removal," Adv. Mater. Technol. **4**, 1800636 (2019).
[21]M. Zarei and M. Zarei, "Self-propelled micro/nanomotors for sensing and environmental remediation," Small **14**, 1800912 (2018).
[22]I. Tiwari, P. Parmananda, and R. Chelakkot, "Periodic oscillations in a string of camphor infused disks," Soft Matter **16**, 10334–10344 (2020).
[23]R. Fujita, M. Matsuo, and S. Nakata, "Multidimensional self-propelled motion based on nonlinear science," Front. Phys. , 128 (2022).
[24]T. Mitsumata, J. P. Gong, and Y. Osada, "Shape memory functions and motility of amphiphilic polymer gels," Polym. Adv. Technol. **12**, 136–150 (2001).
[25]R. Sharma, S. T. Chang, and O. D. Velev, "Gel-based self-propelling particles get programmed to dance," Langmuir **28**, 10128–10135 (2012).
[26]N. Bassik, B. T. Abebe, and D. H. Gracias, "Solvent driven motion of lithographically fabricated gels," Langmuir **24**, 12158–12163 (2008).
[27]L. Keiser, H. Bense, P. Colinet, J. Bico, and E. Reyssat, "Marangoni bursting: evaporation-induced emulsification of binary mixtures on a liquid layer," Phys. Rev. Lett. **118**, 074504 (2017).
[28]K. H. Nagai, K. Tachibana, Y. Tobe, M. Kazama, H. Kitahata, S. Omata, and M. Nagayama, "Mathematical model for self-propelled droplets driven by interfacial tension," J. Chem. Phys. **144**, 114707 (2016).
[29]V. Pimienta, M. Brost, N. Kovalchuk, S. Bresch, and O. Steinbock, "Complex shapes and dynamics of dissolving drops of dichloromethane," Angew. Chem. Int. Ed. **50**, 10728–10731 (2011).
[30]K. Nagai, Y. Sumino, H. Kitahata, and K. Yoshikawa, "Mode selection in the spontaneous motion of an alcohol droplet," Phys. Rev. E **71**, 065301 (2005).
[31]A. Nikolov, D. Wasan, and J. Lee, "Tears of wine: The dance of the droplets," Adv. Colloid Interface Sci. **256**, 94–100 (2018).
[32]C. Spandagos, T. B. Goudoulas, P. F. Luckham, and O. K. Matar, "Surface tension-induced gel fracture. part 1. fracture of agar gels," Langmuir **28**, 7197–7211 (2012).
[33]M. Okada, Y. Sumino, H. Ito, and H. Kitahata, "Spontaneous deformation and fission of oil droplets on an aqueous surfactant solution," Phys. Rev. E **102**, 042603 (2020).
[34]Y. Sumino, H. Kitahata, H. Seto, and K. Yoshikawa, "Blebbing dynamics in an oil-water-surfactant system through the generation and destruction of a gel-like structure," Phys. Rev. E **76**, 055202 (2007).
[35]Y. Sumino, H. Kitahata, Y. Shinohara, N. L. Yamada, and H. Seto, "Formation of a multiscale aggregate structure through spontaneous blebbing of an interface," Langmuir **28**, 3378–3384 (2012).
[36]Y. Sumino, H. Kitahata, H. Seto, and K. Yoshikawa, "Dynamical blebbing at a droplet interface driven by instability in elastic stress: a novel self-motile system," Soft Matter **7**, 3204–3212 (2011).
[37]V. S. Akella, D. K. Singh, S. Mandre, and M. M. Bandi, "Dynamics of a camphoric acid boat at the air–water interface," Phys. Lett. A **382**, 1176–1180 (2018).
[38]J. Nie, W. Lu, J. Ma, L. Yang, Z. Wang, A. Qin, and Q. Hu, "Orientation in multi-layer chitosan hydrogel: morphology, mechanism and design principle," Sci. Rep. **5**, 1–7 (2015).
[39]P. Kumar, D. Sebők, Á. Kukovecz, D. Horváth, and Á. Tóth, "Hierarchical self-assembly of metal-ion-modulated chitosan tubules," Langmuir **37**, 12690–12696 (2021).

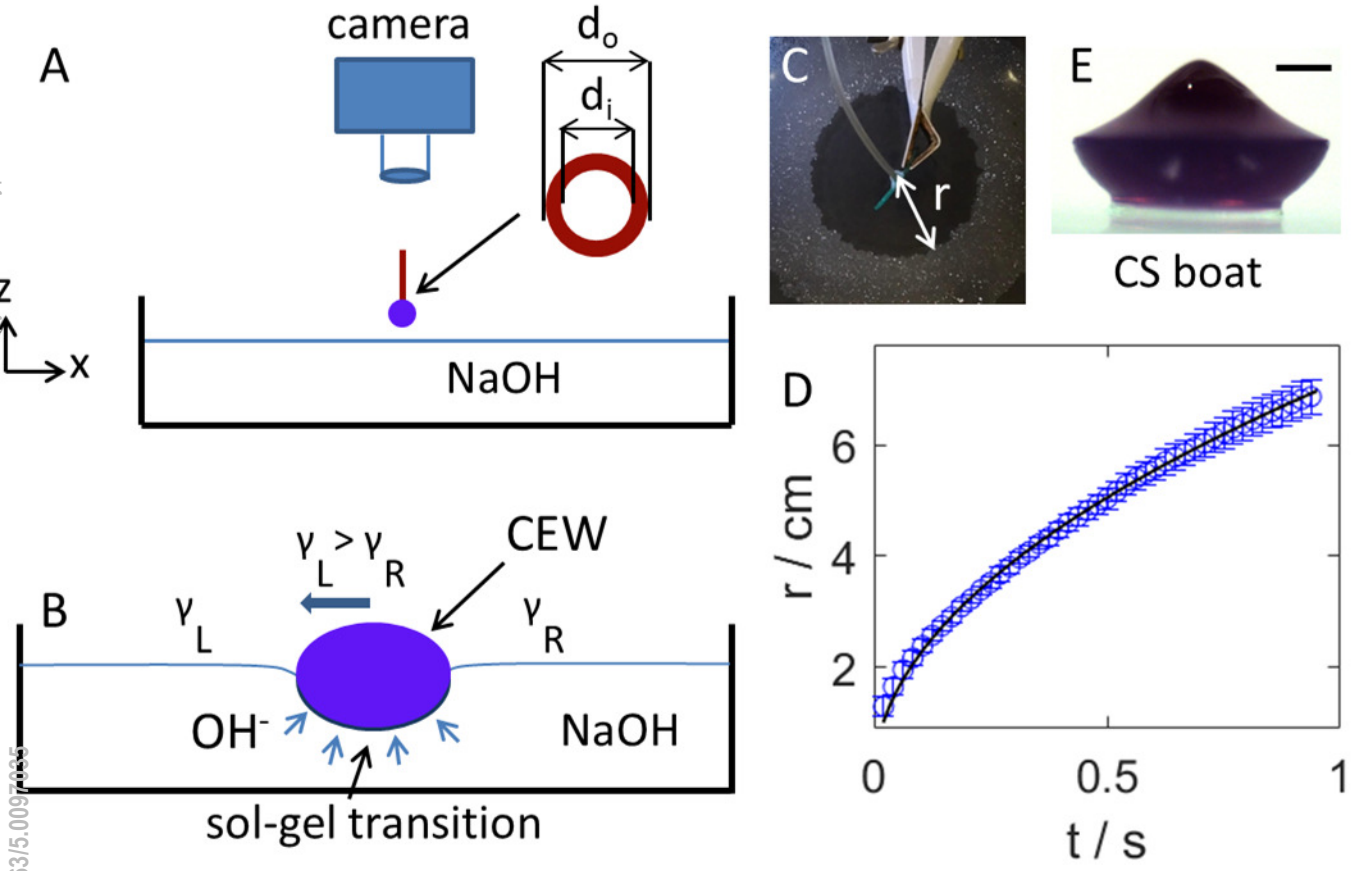

PLEASE CITE THIS ARTICLE AS DOI: 10.1063/5.0097035